IOP Publishing Superconductor Science and Technology
Supercond. Sci. Technol. **27** (2014) 035003 (10pp) doi:10.1088/0953-2048/27/3/035003

Concept of a current flow diverter for accelerating the normal zone propagation velocity in 2G HTS coated conductors

Christian Lacroix and Frederic Sirois

Department of Electrical Engineering, Polytechnique Montréal, Montréal, QC, H3C 3A7, Canada

E-mail: christian.lacroix@polymtl.ca

Received 15 October 2013, revised 25 November 2013
Accepted for publication 17 December 2013
Published 22 January 2014

Abstract

In this paper, we propose a slight change in the architecture of second generation (2G) high temperature superconductor (HTS) coated conductors (CCs), in order to accelerate their normal zone propagation velocity (NZPV) and reduce the probability of developing hot spots. The concept described in this work is to insert a highly resistive layer (called a 'current flow diverter', CFD) at the superconductor–stabilizer interface of the 2G HTS CC. The CFD partially covers this interface, so when a normal zone appears the current that transfers from the superconducting layer to the metallic (stabilizer) layers is forced to circumvent the CFD in order to follow the path of least resistance. This results in a significant increase of the current transfer length and a better spatial distribution of heat generation, that help in increasing the NZPV. According to the numerical model developed in this paper, the CFD architecture allows us to obtain NZPV values of more than 20 m s^{-1}, which is approximately two orders of magnitude faster than what has been measured so far on commercially available 2G HTS CCs. Furthermore, our calculations reveal that, for the same value of interfacial resistance, a tape with the CFD architecture can exhibit an NZPV more than 40 times higher than in the case of a similar tape with a uniform interfacial resistance.

Keywords: coated conductors, high temperature superconductors, quench, normal zone propagation velocity, hot spot

(Some figures may appear in colour only in the online journal)

1. Introduction

Second generation (2G) high temperature superconductor (HTS) coated conductors (CCs) are currently used in the development of numerous high power devices, such as superconducting cables, superconducting transformers, superconducting magnetic energy storage systems, superconducting fault current limiters (SFCLs), superconducting electromagnets, superconducting motors, etc. Among the issues that remain to be solved, that of hot spots following a quench still draw the attention of several research groups. The problem is currently being addressed both from a theoretical/modeling [1–4] and experimental [5–9] point of view.

When the applied current is close or equal to the critical current I_c, thermal instabilities (hot spots) can appear in weaker zones (lower I_c) of a superconducting tape. A zone with a lower I_c can be present because of inhomogeneities (defects) along the length of the tape, which originate from the fabrication process (approximately $\pm 10\%$ of local variations in I_c), or any other phenomena that may increase momentarily the superconductor temperature at a specific point [10, 11]. Hot spots can be very damaging and can even lead to a complete local destruction of the tape. From an application point of view, it is critical to avoid the appearance of hot spots in order to prevent the deterioration of the device.

Hot spot issues exist in all devices based on 2G HTS CCs, but they are more critical for SFCLs, since their main functionality is based on the quench of the superconductor [12, 13], and for superconducting magnets, since their operating

current is generally chosen as close as possible to I_c in order to maximize the generated field [14]. It has been observed many times that 2G HTS CCs have a low normal zone propagation velocity (NZPV), which makes them prone to hot spots. As a result, the temperature of the initial normal zone can increase drastically before a sufficient voltage drop develops and allows either limiting the current (in the case of SFCLs [12]) or detecting the quench (in the case of superconducting electromagnets [15]).

The most common strategy adopted so far to mitigate hot spots has been to increase the thickness of the stabilizer and/or substrate in order to increase the thermal mass [1]. However, this approach reduces the fault current limitation capability of the tape, and makes SFCLs more costly since more stabilizer (e.g. silver) is required, but worst of all it may easily double the total length of tape for a given limitation threshold. In the case of superconducting magnets, besides over-stabilizing the tape with a thick copper shunt, a certain current (or temperature) margin must be used in order to give more time to detect the quench and stop the current supply before the tape is destroyed. This margin obviously reduces the maximum achievable field [14].

Another approach to mitigate the maximum temperature rise at hot spots is to increase the NZPV. The drawback of increasing the NZPV is a decrease of the stability margin of the tape, which is often quantified by the minimum amount of thermal energy required to initiate a quench, more commonly called 'minimum quench energy' (MQE) [6, 16]. However, from an application point of view, there is always a compromise to make between the reduction of the stability margin (i.e. *deliberate increase* of the quench probability) versus the capital investment required to protect the device (i.e. *reduction* of the risk of destroying the tape). The optimal compromise is highly application dependent.

Several solutions have been proposed in order to increase the NZPV in coated conductors. For instance, modifying the substrate thermal and electrical properties by using sapphire instead of Hastelloy increases the NZPV [17]. A second solution to increase the NZPV is to modify the tape architecture itself. As an example, it has been proposed to use a discontinuous contact along the length of the tape between the superconductor and the substrate [18].

More recently, it has been suggested to deliberately increase the interfacial resistance between the superconductor and the stabilizer in order to increase the NZPV in 2G HTS CCs (see [19, 20] and references therein). Doing so increases the current transfer length (CTL) between the superconductor and the stabilizer. Knowing that the NZPV is roughly proportional to the longest length between the CTL and the thermal diffusion length (TDL), it is only necessary to choose a sufficiently high interfacial resistance so that CTL > TDL, and therefore adjust the NZPV as desired. This principle has been experimentally demonstrated in [21] on modified commercial tapes. In particular, NZPV values up to 10 m s^{-1} were reported, which is approximately 25–100 times faster than the 10–40 cm s^{-1} usually measured on commercial tapes.

The simplicity of this solution makes it very attractive, since it is easy to implement. However, the major drawback of an increased interfacial resistance is that the heat generated in the interface at the current lead connections is likely to be much too high for practical purposes, resulting in an unacceptable risk of quench at the contacts.

In this paper, we propose to use a simple tape architecture that allows a significant increase of the CTL, while keeping a relatively low interfacial resistance. In our proposed architecture, the interfacial resistance is not uniform along the tape width, but it is instead constituted of a section of very high resistance (later on called a 'current flow diverter'), and at least one section of very low resistance. The NZPV and CTL of 2G HTS CCs based on this architecture were evaluated with the help of 3D finite element simulations. Comparisons were made for various interfacial resistances, taking the uniform interfacial resistance case as the reference. Our results confirmed that, for the same value of interfacial resistance, the CTL and the NZPV of a tape comprising a 'current flow diverter' can be much higher than that of a tape with uniform interfacial resistance. This is supported by recent experimental measurements realized on modified commercial 2G HTS CCs [22].

2. Finite element electro-thermal model

The 3D finite element simulations performed in this paper were realized with the help of the Joule heating module of the COMSOL Multiphysics 4.3 software package. In this section, we first describe the tape geometry and materials parameters used in the calculations. Then, we present the equations used to model the electrical and thermal behaviors of the simulated tapes.

2.1. Simulation parameters

The tape geometries used in the simulations are presented in figure 1 (not to scale). In figure 1(a), the cross-section of a tape with a uniform interfacial resistance is represented. It consists of a superconducting layer (white) and buffer layers (yellow) deposited on a substrate (brown). All those layers are surrounded by a layer of stabilizer (gray). The interfacial layer between the superconductor and the stabilizer is also included in the drawing (green). The black arrow represents a virtual probe.

An example of the cross-section of a current flow diverter tape is shown in figure 1(b). The only difference is that a layer of high electrical resistivity (blue), that we shall call a 'current flow diverter' (or simply 'CFD'), is inserted at the superconductor–stabilizer interface. The CFD covers only partially the interface (middle of the tape). The rest of the interface (green) remains identical to the interfacial resistance that is found in commercial tapes. The exact dimensions used in the simulations are presented in table 1.

The following materials were used in the simulations: Ag as the stabilizer, MgO as the buffer layers, (RE)BaCuO as the superconducting layer and Hastelloy as the substrate. Most of the physical parameters of the materials used in the simulations can be found in the literature. In this case, the temperature dependence of the thermal conductivity, the heat capacity

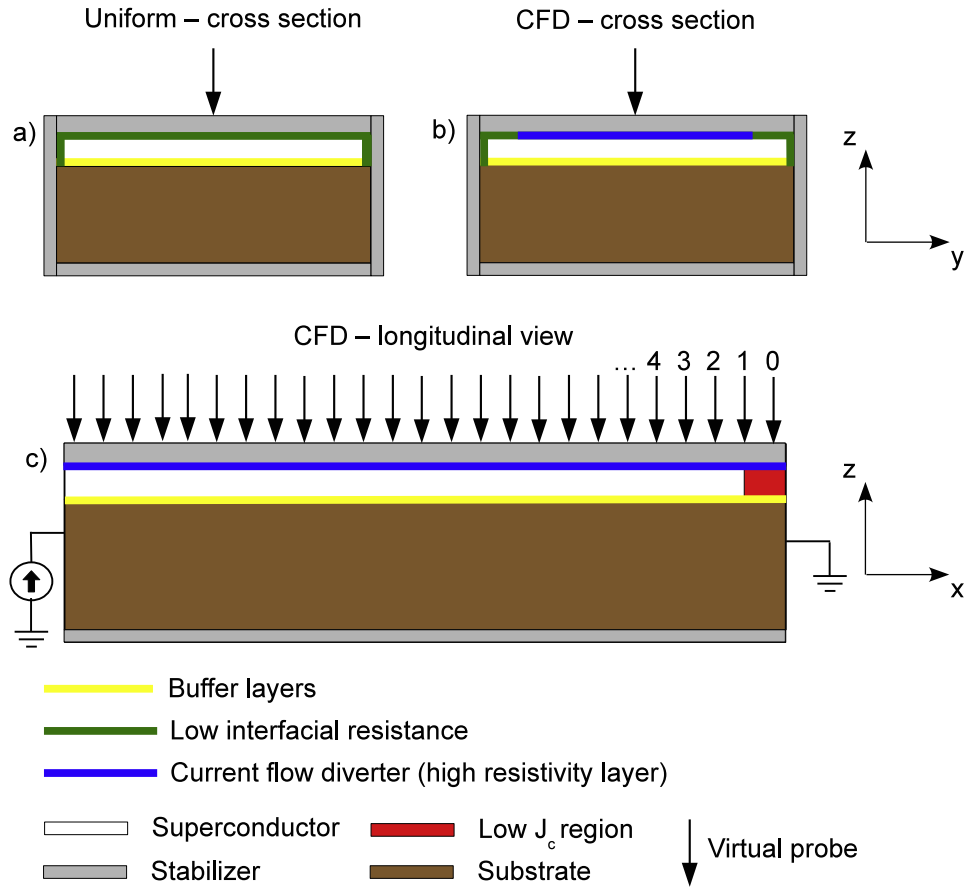

Figure 1. Tape geometries used in finite element calculations (not to scale): (a) cross-section view of a tape with a uniform interfacial resistance; (b) cross-section view of a CFD tape and (c) longitudinal view of a CFD tape with a low J_c region at one end. The numbers are used to distinguish each virtual probe.

Table 1. Geometrical parameters of the simulated tapes.

Parameter	Numerical value
Length	5 cm
Width	1 cm
Substrate thickness	50 μm
Buffer layer thickness	150 nm
Superconductor layer thickness	1 μm
Interfacial layer between superconductor and stabilizer thickness	100 nm
CFD thickness	100 nm
Stabilizer thickness—top	2 μm
Stabilizer thickness—sides and bottom	1 μm

and the electrical conductivity of Ag, MgO, (RE)BaCuO (for $T > T_c$) and Hastelloy were taken from [23–28].

In the case of (RE)BaCuO ($T < T_c$), the electrical behavior is highly non-linear, and reliable data for (RE)BaCuO in 2G HTS CCs over a wide range of temperature and electric field are not available in the literature. However, the electrical conductivity of (RE)BaCuO (σ_{REBCO}) can be reasonably well approximated by using a power-law model in the flux creep and flux flow regimes (σ_{sc}), while the transition from the superconducting state to the normal state (σ_n) can be modeled assuming two resistances in parallel.

In our simulations, the following equations were used:

$$\sigma_{REBCO}(T) = \sigma_{sc}(T) + \sigma_n(T) \tag{1}$$

$$\sigma_{sc}(T) = \frac{J_c(T)}{E_0}\left(\frac{\|E\|}{E_0}\right)^{\frac{1-n(T)}{n(T)}} \tag{2}$$

$$J_c(T) = \begin{cases} J_{c0}\left(\frac{T_c - T}{T_c - T_0}\right) & \text{for } T < T_c \\ 0 & \text{for } T_c \leq T \end{cases} \tag{3}$$

$$n(T) = \begin{cases} (n_0 - 1)\left(\frac{T_c - T}{T_c - T_0}\right)^{1/4} + 1 & \text{for } T < T_c \\ 1 & \text{for } T_c \leq T \end{cases} \tag{4}$$

where T_0 is the liquid nitrogen temperature, J_{c0} is the critical current density at T_0, T_c is the critical temperature, $\|E\|$ is the norm of the electric field, E_0 is the critical electric field and

Table 2. (RE)BaCuO parameters.

Parameter	Numerical value
Critical current density at $T = T_0$ (J_{c0})	3.125 MA cm^{-2}
Critical temperature (T_c)	90 K
Liquid nitrogen temperature (T_0)	77 K
Critical electric field (E_0)	1 μV cm^{-1}
n-parameter at $T = T_0$ (n_0)	13
Defect amplitude (A)	0.75
Defect size (d)	1 mm

n_0 is a fitting parameter. All (RE)BaCuO parameters used in this work are presented in table 2.

In figure 1(c), the longitudinal section of a CFD tape is shown. A low J_c region (red) is included at a specific location in the tape in order to initiate a normal zone propagation. The reduction in critical current was included in (3) by making the following substitution:

$$J_{c0} \rightarrow J_{c0}\left[1 - A\mathrm{e}^{\frac{-(x-l)^2}{2d^2}}\right] \tag{5}$$

where A, d and l correspond to the amplitude, width and position of the low J_c region. When a current density higher than $J_{c0}(1-A)$ is flowing in the superconducting layer, heat is generated in this low J_c region, which creates a normal zone that expands with time.

To minimize computational time of this 3D numerical model, the number of elements was reduced by taking advantage of the symmetries of the problem. First, only half of the width of the tape was modeled. Second, the low J_c region was placed at one end of the tape, while the current was injected at the other end.

For each simulation, a ramp of current followed by a plateau of constant current ($I = 0.8I_{c0} = 250$ A, where I_{c0} is the critical current at $T = T_0$) was imposed as transport current in the tape (see figure 2).

2.2. Electro-thermal model

The variables used in the electro-thermal model are the electrical potential V and the temperature T. To describe the electrical part, the following equations were used:

$$\nabla \cdot (-\sigma(T)\nabla V) = 0, \qquad \text{in the tape,} \tag{6}$$

$$\int_\Omega -\mathbf{n} \cdot (-\sigma(T)\nabla V)\,\mathrm{d}S = I(t), \qquad \text{at one end of the tape,} \tag{7}$$

$$V = 0, \qquad \text{at the other end of the tape,} \tag{8}$$

$$\mathbf{n} \cdot \nabla V = 0, \qquad \text{at the remaining boundaries of the tape,} \tag{9}$$

where $\sigma(T)$ is the electrical conductivity, Ω is the surface at one end of the tape, $I(t)$ is the applied transport current and $\mathbf{n}$ is a local unit vector perpendicular to the external surfaces of the tape.

To describe the thermal part, the heat equation was used, which reads

$$\rho_m C_p(T)\frac{\partial T}{\partial t} + \nabla \cdot (-k(T)\nabla T) = Q_j, \qquad \text{in the tape,} \tag{10}$$

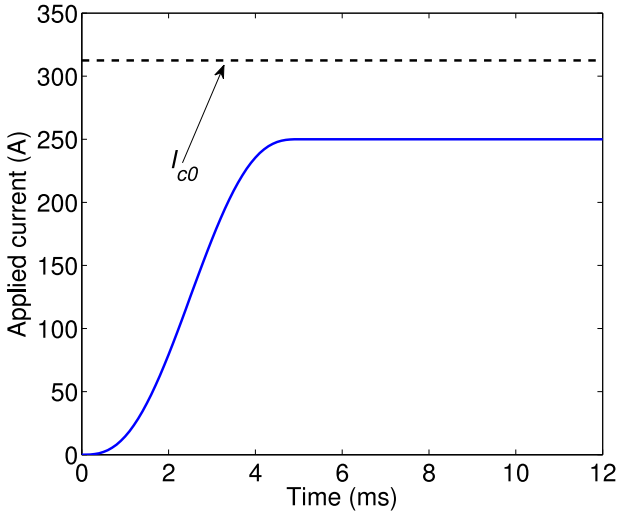

Figure 2. Applied current as a function of time used for all simulations presented in this paper.

where ρ_m is the mass density, $C_p(T)$ is the heat capacity, $k(T)$ is the thermal conductivity and Q_j represent the Joule losses, which ensure the coupling between (6) and (10) through the following expression:

$$Q_j = \sigma(T)(-\nabla V)^2, \qquad \text{in the tape.} \tag{11}$$

At both ends of the tape, we consider that the temperature gradient is zero, which is expressed as

$$\mathbf{n} \cdot \nabla T = 0, \qquad \text{at both ends of the tape.} \tag{12}$$

For the remaining boundaries, we used the following term, which represents the cooling power of liquid nitrogen:

$$\mathbf{n} \cdot (k\nabla T) = h(T - T_0), \qquad \text{at the remaining boundaries,} \tag{13}$$

where h is a heat transfer coefficient representing the thermal exchange from the tape boundaries with the liquid nitrogen [29]. It is worth noting that the effect of this thermal exchange on the results presented below is small and does not affect the main conclusions of this work. It has been considered for the sake of completeness.

2.3. Numerical approximations

To further reduce the computational time, the buffer layers and the interfacial resistance layer were approximated as 2D domains, i.e. as if they were infinitely thin. This approximation implies that the in-plane components of current density (J_x and J_y) are negligible in these layers, and only the normal component remains (J_z). Therefore, (6) becomes a one-dimensional equation, which gives

$$J_z = \sigma(T)\frac{\partial V}{\partial z} = \sigma(T)\left(\frac{V_2 - V_1}{t}\right) \tag{14}$$

where V_2 and V_1 are the electric potentials on each side of the infinitely thin layer, and $\sigma(T)$ and t are the electrical conductivity and thickness of the thin layer, respectively.

Similarly, one can calculate the heat flux (Q_z) flowing through the infinitely thin layers using the following approximation:

$$Q_z = k(T)\frac{\partial T_1}{\partial z} = k(T)\left(\frac{T_2 - T_1}{t}\right) \tag{15}$$

where T_2 and T_1 are the temperatures on each side of the infinitely thin layer and $k(T)$ is the layer thermal conductivity.

We note that, in these approximations, both the electric potential and the temperature are discontinuous in the infinitely thin layer. In other words, the values of the potential and temperature are not the same on both sides of the layer. The jump in their values is handled through the interface boundary conditions (14) and (15), which represents a lumped approximation of the continuous case. This lumped approximation depends on the material properties of the thin layer, i.e. t, $\sigma(T)$ and $k(T)$.

3. Results and discussion

The quench dynamics in 2G HTS CCs with and without a CFD was simulated using the equations described above. We first present and compare results obtained for a tape with a uniform interfacial resistance, that we shall call a 'uniform tape', and for a CFD tape. Then, we compare the dependences of the NZPV and CTL on the interfacial resistance for both architectures. Finally, we discuss of the effect of the CFD interfacial resistance on the NZPV.

3.1. Uniform tape versus CFD tape

Calculations were realized on tapes with an interfacial resistance R_i ranging from 0.01 to 100 $\mu\Omega$ cm^2. In the case of a uniform tape, we considered that the interfacial layer (green line in figure 1(a)) had a thickness of 100 nm. To vary the interfacial resistance, the resistivity of the interfacial layer was varied from 0.001 to 10 Ω cm.

In a CFD tape, the low resistance part of the interfacial layer (green line in figure 1(b)) was set to a constant value of $R_i^* = 100$ nΩ cm^2. For the high resistance part of the interfacial layer (blue line in figure 1(b)), which corresponds to the CFD itself, calculations were realized for CFDs with different widths w_f and interfacial resistances R_f. Note that the thickness of the CFD was fixed to 100 nm for all calculations.

In the case where $R_f \gg R_i^*$, i.e. the interfacial resistance of the CFD (R_f) is much higher than the intrinsically low interfacial resistance existing between the superconducting and stabilizer layer (R_i^*), the resulting interfacial resistance is given by

$$R_i \approx \frac{R_i^*}{(1-f)}, \tag{16}$$

where $R_i^* = 100$ nΩ cm^2, $f = w_f/w_t$ is the coverage fraction of the CFD and w_t is the total width of the tape. For example, if the CFD covers 90% of the interface ($f = 0.9$), we obtain $R_i \approx 1$ $\mu\Omega$ cm^2.

In figure 3(a), the variation in time of the electric fields, obtained from virtual probes located on the top of the stabilizer and separated by a distance of 1 mm (see figure 1), is presented in the case of a uniform tape with $R_i = 1$ $\mu\Omega$ cm^2, in which a constant current of 250 A is applied. Also, the variation in time of the temperatures obtained at the same virtual probe locations is presented in figure 3(c).

The variation in time of the electric field is similar to what was observed from experiments (for instance, see [21]). When time increases, the first measurable electric field appears at the probe where the low J_c region is located, then at the closest probe to the low J_c region, then the second closest, and so on. For each curve, we observe that the electrical field first increases non-linearly, then when it reaches a value between 35 and 45 V m^{-1} the rising rate suddenly decreases and remains almost constant for the rest of the simulation. The change in the slope corresponds approximately to the instant at which the current has completely transferred from the superconductor to the stabilizer, which is confirmed on the temperature plot by noticing that the temperature reaches T_c at approximately the same time instant (see figure 3(c)).

Given that all curves are parallel to each other (except curves 0 and 1), the NZPV can be calculated by dividing the distance between two virtual probes by the time elapsed to reach the same electric field or temperature. According to figures 3(a) and (c), the NZPV is 18.8 cm s^{-1}.

Figure 3(b) shows the time evolution of the electric field in a CFD tape. In that case, $R_f = 1$ Ω cm^2 and $f = 0.9$, which gives a global interfacial resistance of $R_i = 1$ $\mu\Omega$ cm^2. The time evolution of the temperature measured at the same probes is shown in figure 3(d). It is worth emphasizing that the time evolution of the electric field and temperature is quite different in comparison with the uniform case. As seen in the insets, for the CFD tape, the curves are much closer to each other, indicating that the propagation of the normal zone occurs much faster. In the particular case of this simulation, a NZPV of 736 cm s^{-1} was found, which is approximately 40 times faster than for a uniform tape with the same interfacial resistance.

Figure 4(a) shows the temperature distribution on top of the silver stabilizer at time $t = 10$ ms for a uniform tape ($R_i = 1$ $\mu\Omega$ cm^2). We observe that the temperature gradient is almost zero along the width of the tape except at the edge of the tape (lower boundary), where the current is slightly more concentrated due to the presence of the lateral silver coating (see figure 1), which introduces a small 3D effect.

Figure 4(b) presents the temperature distribution on top of the silver stabilizer at time $t = 10$ ms for a CFD tape ($R_f = 1$ Ω cm^2 and $f = 0.9$) with the same global interfacial resistivity ($R_i = 1$ $\mu\Omega$ cm^2). We observe that the temperature gradient is almost zero along the width of the tape, except at the edge of the CFD, where it increases drastically. This suggests that, when the current transfers from the superconductor to the stabilizer, it concentrates at the edges of the CFD, which generates a local excess of heat that increases the temperature at this location, and which in turn accelerates the NZPV.

The transfer of the current from the superconductor to the stabilizer at the frontier between the superconducting and the

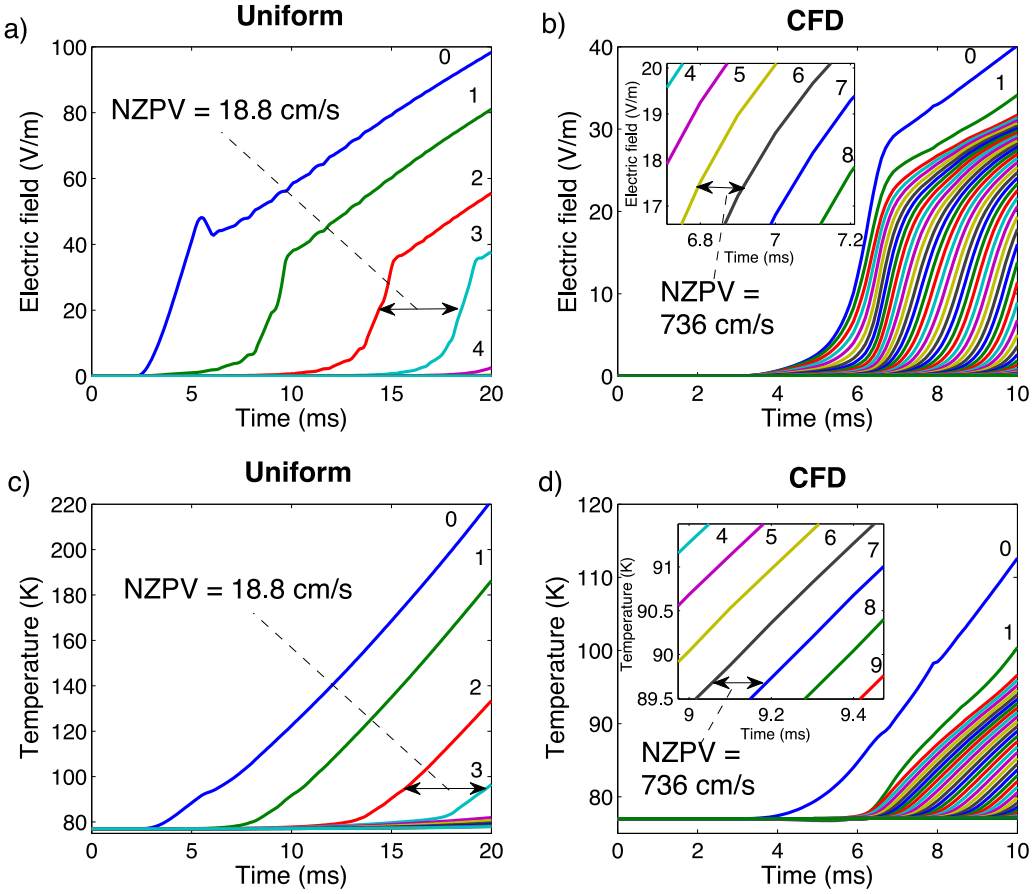

Figure 3. Time evolution of the electric field for (a) a uniform tape and (b) a CFD tape, and of the temperature for (c) a uniform tape and (d) a CFD tape, measured at the virtual probes located on top of the stabilizer (superconductor side), along the center line of the tape, as shown in figure 1(c). Each line represents the electric field or temperature measured by a virtual probe (see figure 1). Probe '0' is located on top of the low J_c region. The distance between the virtual probes is 1 mm. The interfacial resistance R_i for both tapes is 1 $\mu\Omega$ cm^2. For the CFD tape, $R_f = 1\ \Omega$ cm^2 and $f = 0.9$ (the CFD covers 90% of the interface). Insets: zoom of the electric field and temperature curves close to the superconducting to normal transition for the CFD tape.

normal zones is presented in figure 5, where both the current in the superconductor (red arrows) and in the stabilizer (blue arrows) are shown for a uniform and a CFD tape. Both tapes (uniform and CFD) are identical to the ones from figure 4. The color plot represents the current density in the stabilizer. In the case of a uniform tape, the current flows mostly in the x direction except at the edge of the tape. We observe that the transition is quite sharp in comparison with the CFD tape, where a certain amount of current can exist simultaneously in both layers over a considerable length. We also clearly see that the CFD tape forces the current to transfer via the edges of the tape (the only path to circumvent the highly resistive interface), which is not the case for a uniform tape.

In figure 6, the spatial variation (x-direction) of the current in the metallic layers divided by the total current obtained at time $t = 8.3$ ms is presented for three architectures having a global interfacial resistance of 1 $\mu\Omega$ cm^2: a uniform tape, a low resistance CFD tape ($R_f = 100\ \mu\Omega$ cm^2 and $f = 0.9$) and a high resistance CFD tape ($R_f = 1\ \Omega$ cm^2 and $f = 0.9$). We observe that, in the case of the uniform tape and low resistance CFD tape, the current transfer along the tape length follows an exponential path ($I \propto e^{-x/\lambda}$), where λ is a characteristic length that is defined as the current transfer length (CTL) in the literature [30]. In other words, the CTL classically corresponds to the distance required for a given injected current to drop by a factor of e^1.

In the case of the high resistance CFD tape, the current transfer does not follow an exponential function but rather looks like the logistic function ($I \propto \frac{1}{1+e^{x/\lambda}}$). Because of this fundamental difference, we used the following criterion instead of the exponential one in order to determine the CTL for all cases: the CTL is defined as the distance required for the current to pass from 10% to 90% of its total value in the metallic layers. In the cases illustrated in figure 6, this represents values of 0.8, 5.5 and 12.0 mm for the uniform tape, the low resistance CFD tape and the high resistance CFD tape, respectively. This suggests that the high NZPV observed in the CFD tape is correlated to its high CTL.

It is interesting to note that this high CTL results from a purely geometrical effect. Indeed, as can be seen in the simplified schematic of figure 7, the CFD forces the current to pass through a specific path upon its transfer from the superconducting layer to the stabilizer layer. Since this transfer occurs over a longer distance than in a uniform tape, the CTL

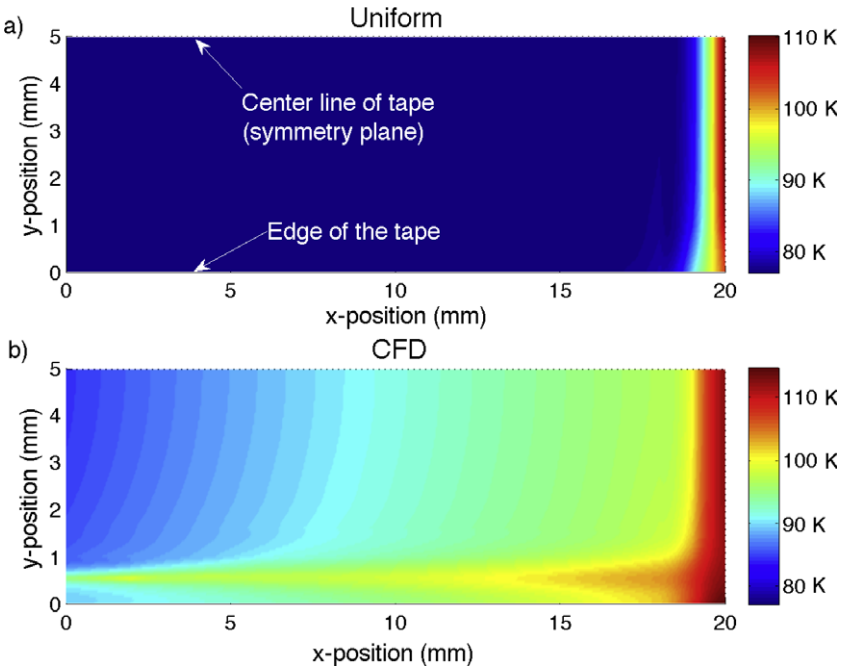

Figure 4. Two-dimensional contour maps of the spatial variation of the temperature on top of the tape (HTS side) obtained at $t = 10$ ms for (a) a uniform tape and (b) a CFD tape ($R_f = 1\ \Omega\ \mathrm{cm}^2$ and $f = 0.9$). Both tapes have an interfacial resistance $R_\mathrm{i} = 1 \mu\Omega\ \mathrm{cm}^2$. Only the half-width of the tape is represented.

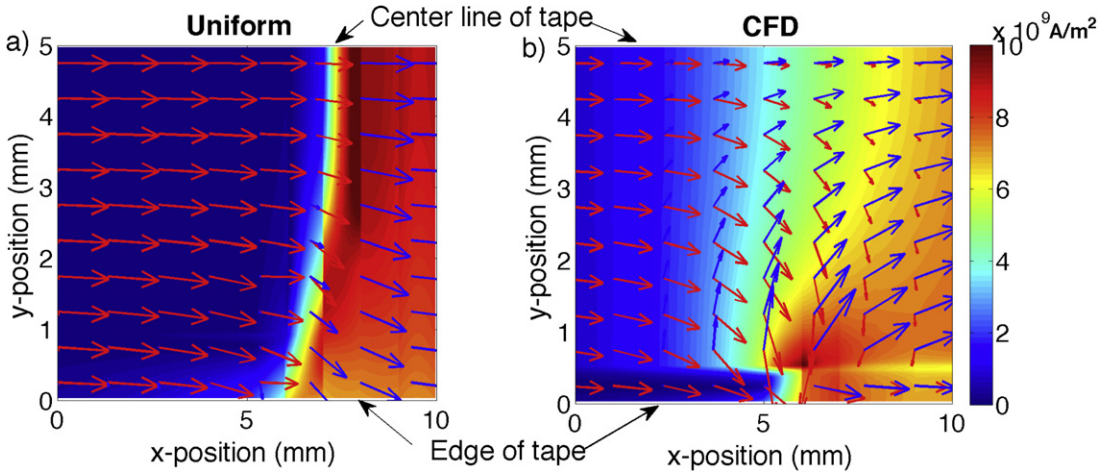

Figure 5. Two-dimensional current distribution of the current density in the stabilizer (top view of the tape) at the frontier between the superconducting and normal zones for (a) a uniform tape and (b) a CFD tape ($R_f = 1\ \Omega\ \mathrm{cm}^2$ and $f = 0.9$). Both tapes have an interfacial resistance $R_\mathrm{i} = 1\ \mu\Omega\ \mathrm{cm}^2$. The red and blue arrows represent the current density in the superconductor and in the stabilizer respectively. Only the half-width of the tape is represented.

is artificially increased. Therefore, the length over which the heat is generated in front of the moving quench boundary is longer, which accelerates the NZPV.

3.2. Dependence of NZPV and CTL on parameters

The dependence of the NZPV on the global interfacial resistance of the tape R_i was investigated. For the uniform case, the resistivity of the interfacial resistance layer was varied. For the CFD case, the coverage fraction f was used to vary R_i. The results are presented in figure 8. We observe that, in the case of a uniform tape, the NZPV is constant for $R_\mathrm{i} < 0.1\ \mu\Omega\ \mathrm{cm}^2$. In that regime, the NZPV is dominated by the thermal diffusion in the substrate, as described in [19]. If R_i is between 0.1 and 1 $\mu\Omega\ \mathrm{cm}^2$, the thermal diffusion length and the CTL are of the same order of magnitude. When $R_\mathrm{i} > 1\ \mu\Omega\ \mathrm{cm}^2$, the dominating length is the CTL and the NZPV increases rapidly with R_i. The uniform interfacial resistance architecture thus allows an increase of the NZPV only when the interfacial resistance is sufficiently high. However, such a high interfacial resistance is unsuitable for making good current

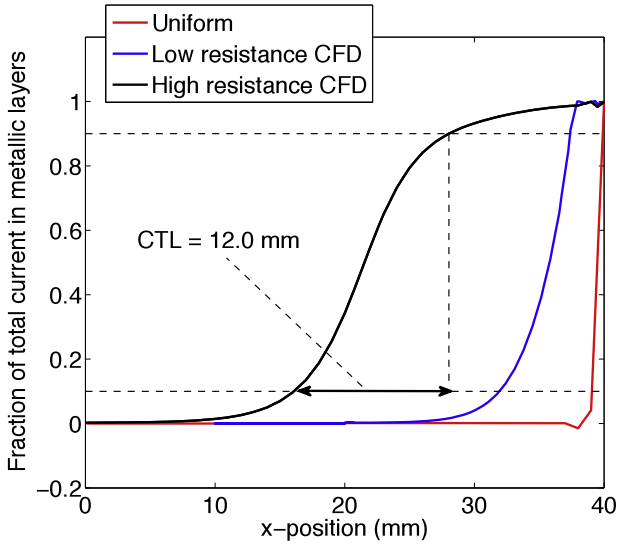

Figure 6. Spatial variation of the normalized current in the metallic layers at $t = 8.3$ ms for three architectures having the same interfacial resistance ($R_\mathrm{i} = 1\ \mu\Omega\ \mathrm{cm}^2$): a uniform tape, a low resistance CFD tape ($R_f = 100\ \mu\Omega\ \mathrm{cm}^2$ and $f = 0.9$) and a high resistance CFD tape ($R_f = 1\ \Omega\ \mathrm{cm}^2$ and $f = 0.9$). At $x = 40$ mm, all current flows in the metallic layers. The dashed lines correspond to the situations where 90% of the total current is in the metallic layers or in the superconductor.

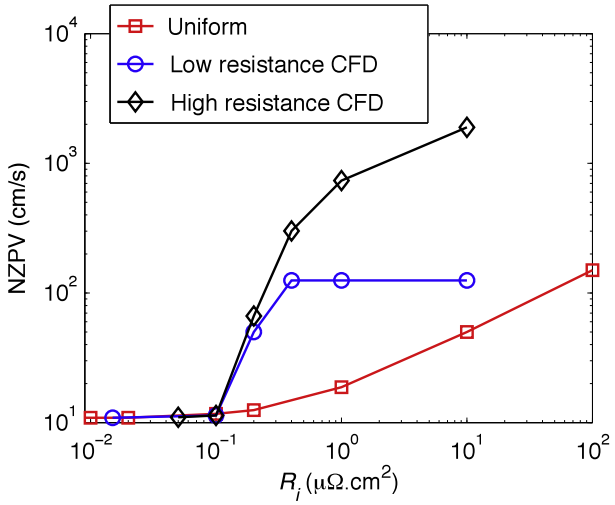

Figure 8. Dependence of the NZPV on the interfacial resistance for a uniform tape, a low resistance CFD tape ($R_f = 100\ \mu\Omega\ \mathrm{cm}^2$ and $f = 0.9$) and a high resistance CFD tape ($R_f = 1\ \Omega\ \mathrm{cm}^2$ and $f = 0.9$).

lead connections, since significant heat will be generated at the contacts, which is likely to lead to contact failures.

For the CFD architecture, and remembering that for these calculations R_i in the CFD architecture is solely a function of the coverage fraction f as per equation (16), the NZPV increases much more rapidly for the same increase of R_i. In the case of a low resistance CFD tape ($R_f = 100\ \mu\Omega\ \mathrm{cm}^2$), the NZPV saturates at 125 cm s^{-1} when R_i reaches 0.4 $\mu\Omega\ \mathrm{cm}^2$. This is an expected behavior since this case corresponds to the NPZV of a tape whose CFD covers 100% of the interface, which is degenerate to the case of a uniform tape architecture with $R_\mathrm{i} = 100\ \mu\Omega\ \mathrm{cm}^2$. In the case of a high resistance CFD tape ($R_f = 1\ \Omega\ \mathrm{cm}^2$), the NZPV increases non-linearly but steadily (no saturation observed) and can reach values higher than 20 m s^{-1} when $R_\mathrm{i} > 10\ \mu\Omega\ \mathrm{cm}^2$ or more.

Figure 9 presents the dependence of the CTL on R_i for the same architectures as in figure 8. In comparison with the uniform case, and as observed earlier, the values of CTL obtained with the CFD architectures are much higher for the same R_i. The trends for each architecture are similar to those observed in figure 8, which supports again the idea of a strong correlation between the NZPV and the CTL.

Finally, figure 10 shows the dependence of the NZPV on the CFD interfacial resistance when the CFD covers 90% of the interface ($f = 0.9$). We observe that the NZPV increases non-linearly when R_f increases and reaches a constant value of 736 cm s^{-1} for $R_f = 1\ \Omega\ \mathrm{cm}^2$ or higher. This can be interpreted as follows: as R_f increases, the fraction of current passing through the CFD decreases to almost zero when $R_f > 1\ \Omega\ \mathrm{cm}^2$. Therefore, for very high values of R_f, all current transfers from the superconductor to the metallic layers by the edges

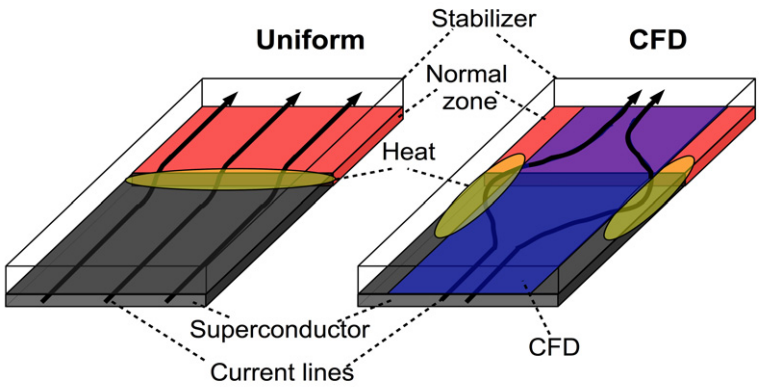

Figure 7. Schematic drawing of the current path flows when the current transfers from the superconductor to the stabilizer to circumvent a normal zone in the case of (i) a uniform tape (left) and (ii) a CFD tape (right). For the sake of simplicity, only the superconducting layer, the CFD and the top part of the stabilizer are represented.

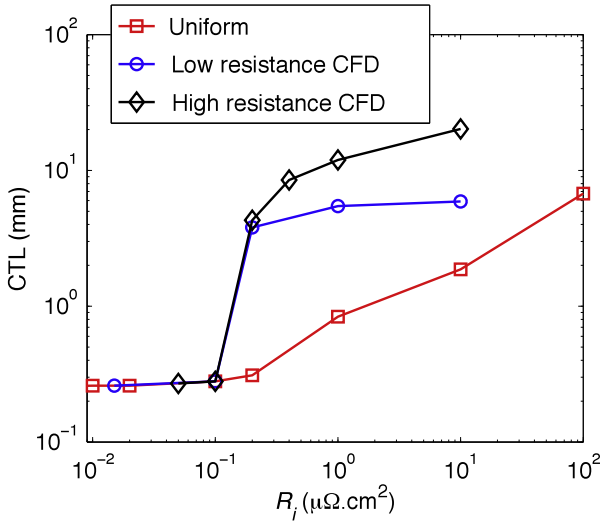

Figure 9. Dependence of the CTL on the interfacial resistance (R_i) for a uniform tape, a low resistance CFD tape ($R_f = 100\ \mu\Omega\ \text{cm}^2$ and $f = 0.9$) and a high resistance CFD tape ($R_f = 1\ \Omega\ \text{cm}^2$ and $f = 0.9$).

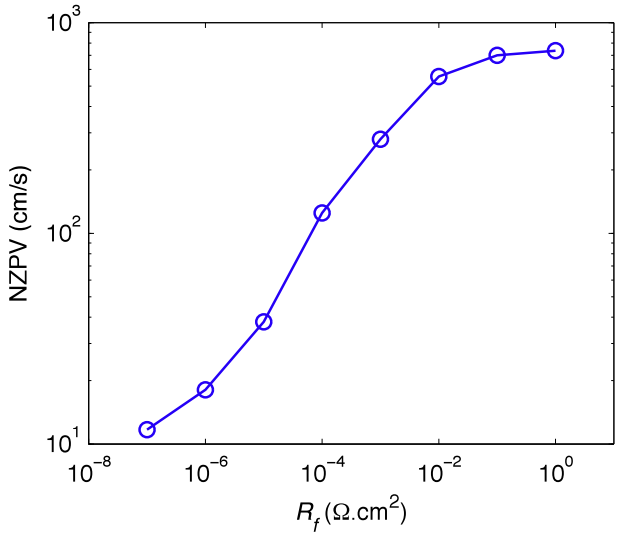

Figure 10. Dependence of the NZPV on the interfacial resistance of the CFD (R_f) in the case where the CFD covers 90% of the superconductor–stabilizer interface ($f = 0.9$).

of the tape, accentuating the effect of current concentration and local heat generation. This suggests that the optimal CFD architecture is the one where R_f is very high.

4. Summary

In this paper, we have introduced a concept of 2G HTS CC tape architecture called a 'current flow diverter' (or simply 'CFD') that allows a significant increase of the NZPV of these tapes, with only a slight increase of the global interfacial resistance (R_i). In the CFD concept, the current is forced to pass at the edges of the tape when it transfers from the superconductor to the metallic layers, which increases the current transfer length (CTL), and at the same time the NZPV, since the two are directly correlated. Our finite element calculations revealed that, for the same value of interfacial resistance, the NZPV of a CFD tape can be increased by a factor of more than 40 in comparison with a uniform tape. To obtain comparable values of NZPV in a uniform tape, a much higher R_i is required, with the consequence of generating an important amount of heat at the current lead connections, which is unacceptable in practice. We expect that the concept described in this work will not present any major issue of implementation by tape manufacturers. Any material that has a sufficiently high resistivity and which is compatible with the fabrication process of 2G HTS CCs could in principle be used as the CFD.

Acknowledgments

The authors are grateful to C-H Bonnard, W K Chan, B Dutoit, F Roy and S Memiaghe for valuable discussions. This work was supported by grants from NSERC (Canada) and FRQNT (Québec), as well as the RQMP infrastructure (Réseau Québécois des Matériaux de Pointe).

References

[1] Fu Y, Tsukamoto O and Furuse M 2003 Copper stabilization of YBCO coated conductor for quench protection *IEEE Trans. Appl. Supercond.* **13** 1780

[2] Chan W K, Masson P J, Luongo C and Schwartz J 2010 Three-dimensional micrometer-scale modeling of quenching in high-aspect-ratio coated conductor tapes part I: model development and validation *IEEE Trans. Appl. Supercond.* **20** 2370

[3] Chan W K and Schwartz J 2011 Three-dimensional micrometer-scale modeling of quenching in high-aspect-ratio coated conductor tapes part II: Influence of geometric and material properties and implications for conductor engineering and magnet design *IEEE Trans. Appl. Supercond.* **21** 3628

[4] Celentano G *et al* 2009 Hot spot stimulated transition in YBCO coated conductors: Experiments and simulations *IEEE Trans. Appl. Supercond.* **19** 2486

[5] Grabovickic R, Lue J W, Gouge M J, Demko J A and Duckworth R C 2003 Measurements of temperature dependence of the stability and quench propagation of a 20-cm-long RABiTS Y–Ba–Cu–O tape *IEEE Trans. Appl. Supercond.* **13** 1726

[6] Wang X, Trociewitz U P and Schwartz J 2007 Near-adiabatic quench experiments on short $YBa_2Cu_3O_{7-\delta}$ coated conductors *J. Appl. Phys.* **101** 053904

[7] Daibo M, Fujita S, Haraguchi M, Iijima Y and Saitoh T 2011 Evaluation of the normal-zone propagation characteristics of REBCO coated conductors with laminated Cu tape *IEEE Trans. Appl. Supercond.* **21** 2428

[8] Tixador P, Cointe Y, Villard C and Usoskin A 2007 Limiting experiments with coated conductors *IEEE Trans. Appl. Supercond.* **17** 3467

[9] Pelegrin J, Martinez E, Angurel L A, Xie Y-Y and Selvamanickam V 2011 Numerical and experimental analysis of normal zone propagation on 2G HTS wires *IEEE Trans. Appl. Supercond.* **21** 3041

[10] Kudymow A, Noe M, Schacherer C, Kinder H and Prusseit Werner 2007 Investigation of YBCO coated

conductor for application in resistive superconducting fault current limiters *IEEE Trans. Appl. Supercond.* **17** 3499
[11] Gurevich A 2001 Thermal instability near planar defects in superconductors *Appl. Phys. Lett.* **78** 1891
[12] Colangelo D and Dutoit B 2012 Inhomogeneity effects in HTS coated conductors used as resistive FCLs in medium voltage grids *Supercond. Sci. Technol.* **25** 095005
[13] Tixador P and Nguyen N T 2012 Design of ReBaCuO-coated conductors for FCL *Supercond. Sci. Technol.* **25** 014009
[14] Awaji S, Hou Y, Oguro H, Watanabe K, Inoue I, Sakamoto H, Yasunaga S and Ryu J 2012 Hot spot behavior of Y123 coated conductors *IEEE Trans. Appl. Supercond.* **22** 6601004
[15] Wang X, Trociewitz U P and Schwartz J 2009 Self-field quench behaviour of $YBa_2Cu_3O_7$ coated conductors with different stabilizers *Supercond. Sci. Technol.* **22** 085005
[16] Dresner L 2002 *Stability of Superconductors* (Dordrecht: Kluwer Academic Publishers)
[17] Antognazza L, Therasse M, Decroux M, Roy F, Dutoit B, Abplanalp M and Fischer O 2009 Comparison between the behavior of HTS thin film grown on sapphire and coated conductors for fault current limiter applications *IEEE Trans. Appl. Supercond.* **19** 1960
[18] Kinder H, Price A and Hiebl A 2006 New mechanism for fast quench propagation in coated conductors *J. Phys.: Conf. Ser.* **43** 146
[19] Levin G A, Novak K A and Barnes P N 2010 The effects of superconductor-stabilizer interfacial resistance on the quench of a current-carrying coated conductor *Supercond. Sci. Technol.* **23** 014021
[20] Levin G A, Jones W A, Novak K A and Barnes P N 2011 The effects of superconductor stabilizer interfacial resistance on quenching of a pancake coil made out of coated conductor *Supercond. Sci. Technol.* **24** 035015
[21] Lacroix C, Fournier-Lupien J-H, McMeekin K and Sirois F 2013 Normal zone propagation velocity in 2G HTS coated conductor with high interfacial resistance *IEEE Trans. Appl. Supercond.* **23** 4701605
[22] Lacroix C, Lapierre Y, Coulombe J and Sirois F 2014 High normal zone propagation velocity in 2G HTS coated conductors with a current flow diverter architecture *Supercond. Sci. Technol.* submitted
[23] Touloukian Y S 1970 *Thermophysical Properties of Matter* (New York: IF/Plenum)
[24] Lide D R 2010 *CRC Handbook of Chemistry and Physics* (New York: CRC Press)
[25] Gordon J E, Fisher R A, Kim S and Phillips N E 1989 Lattice and electronic specific heat of $YBa_2Cu_3O_7$ *Physica* C **162** 484
[26] Hagen S J, Wang Z Z and Ong N P 1989 Anisotropy of the thermal conductivity of $YBa_2Cu_3O_7$ *Phys. Rev.* B **40** 9389
[27] Friedmann T A, Rabin M W, Giapintzakis J, Rice J P and Ginsberg D M 1990 Direct measurement of the anisotropy of the resistivity in the *a–b* plane of twin-free single-crystal superconducting $YBa_2Cu_3O_7$ *Phys. Rev.* B **42** 6217–21
[28] Lu J, Choi E S and Zhou H D 2008 Physical properties of hastelloy®C-276™ at cryogenic temperatures *J. Appl. Phys.* **103** 064908
[29] Roy F, Dutoit B, Grilli F and Sirois F 2008 Magneto-thermal modeling of second-generation HTS for resistive fault current limiter design purposes *IEEE Trans. Appl. Supercond.* **18** 29
[30] Polak M, Zhang W, Parrell J, Cai X Y, Polyanskii A, Hellstrom E E, Larbalestier D C and Majoros M 1997 Current transfer lengths and the origin of linear components in the voltage–current curves of Ag-sheathed BSCCO components *Supercond. Sci. Technol.* **10** 769